JOURNAL OF AIRCRAFT
Vol. 43, No. 1, January–February 2006

Load Alleviation for a Tilt-Rotor Aircraft in Airplane Mode

Binoy Manimala,* Gareth D. Padfield,† and Daniel Walker‡
University of Liverpool, Liverpool, L69 3GH, United Kingdom

Results from research into active structural load alleviation are presented for a tilt-rotor aircraft. The work formed part of the European Commission's Fifth Framework "critical technology" Rotorcraft Handling, Interactions, and Loads Prediction project. Results are presented from an analysis of the structural loads of a tilt-rotor aircraft maneuvering in airplane mode. The potential for suppression of structural loads through active control is assessed. The study has addressed modeling aspects, particularly the nature of the buildup of dynamic loads during maneuvers. The Eurocopter EUROTILT configuration has been used as the test aircraft and a model is developed within the FLIGHTLAB simulation environment. Mathematical analysis and simulation of the rotor in-plane moments and gimbal flapping during longitudinal and lateral maneuvers are presented. The problem also addressed the torque split on the interconnect drive shaft in airplane mode for maneuvers involving large roll and yaw rates. Attempts were made to design an "ideal" controller that minimizes the gimbal flap excursions and the loads using a linear quadratic Gaussian formulation. In this preliminary conceptual study, robustness, actuator requirements, or the availability of measurements were not considered. The main objective of the controller design study was to investigate the effectiveness of cyclic controls to achieve simultaneous suppression of the loads and flapping. Evaluations performed using the controller show that use of cyclic controls is very effective in suppressing the buildup of in-plane loads, gimbal flapping, and interconnect drive shaft torque split.

Nomenclature

a, b	=	longitudinal and lateral gimbal tilts (right rotor, if not specified)
$\dot{a}, \dot{b}$	=	longitudinal and lateral gimbal tilt rates (right rotor, if not specified)
a_1, b_1	=	left-rotor longitudinal and lateral gimbal tilts
a_2, b_2	=	right-rotor longitudinal and lateral gimbal tilts
$\boldsymbol{d}$	=	disturbance vector in linear quadratic Gaussian (LQG) formulation
I_β	=	flap moment of inertia of a rotor blade
$\boldsymbol{J}$	=	cost function in LQG formulation
K_β	=	gimbal spring stiffness
k_1, k_2, k_3	=	constants used in the in-plane moment equation
L	=	lift force at a blade element
$\boldsymbol{m}$	=	measurements in LQG formulation
M_z	=	in-plane moment envelope in multiblade coordinate
$M_{z_{bi}}$	=	in-plane moment of the ith blade in blade axis
P_0, P_1	=	constants in the in-plane load equation
p, q, r	=	fuselage angular velocity components in body axis
$\boldsymbol{Q}, \boldsymbol{R}$	=	weighting matrices in LQG formulation
r_b	=	radial location of a blade element form the rotor hub
T_{htobl}	=	transformation from hub to rotating blade axis
$\boldsymbol{u}$	=	control vector
u, v, w	=	aircraft body axis velocities at the center of gravity
$u^{\text{bl}}, v^{\text{bl}}, w^{\text{bl}}$	=	velocities of a blade element in rotating blade axis
u^h, v^h, w^h	=	velocities at the rotor hub in hub axis
u_t, u_p	=	tangential and normal relative air velocities for a blade element
W_{act}	=	actuator transfer function
$\boldsymbol{x}$	=	state vector in LQG formulation
x_h, y_h, z_h	=	distances of the rotor hub from the vehicle c.g.
$\boldsymbol{y}$	=	output vector for LQG minimization
α	=	angle of attack of a blade element
β	=	blade flap angle
ζ	=	rudder deflection
η	=	elevator deflection
θ_{1c}	=	lateral cyclic pitch
$\theta_{1\text{cd}}$	=	differential lateral cyclic pitch
θ_{1s}	=	longitudinal cyclic pitch
$\theta_{1\text{sd}}$	=	differential longitudinal cyclic pitch
θ_0	=	collective pitch
θ_{0d}	=	differential collective pitch
ξ	=	aileron deflection
Φ	=	rotor inflow angle
ψ	=	blade azimuth
Ω	=	rotor speed
$\boldsymbol{\omega}$	=	angular velocity vector of the fuselage in body axis
$\boldsymbol{\omega}^{\text{bl}}$	=	angular velocity vector of a blade in blade axis
$\omega_x^{\text{bl}}, \omega_y^{\text{bl}}, \omega_z^{\text{bl}}$	=	components of $\boldsymbol{\omega}^{\text{bl}}$
$\omega_x, \omega_y, \omega_z$	=	components of $\boldsymbol{\omega}$

Introduction

IT is anticipated that, during the next few years, tilt-rotor aircraft will enter operational service in both military and civil configurations. A significant amount of research and development work has been carried out in the United States, particularly with the Bell XV-15 research aircraft, leading to the Bell-Boeing V-22 Osprey and the recent initial flight tests of the Bell-Agusta BA609. In response to the expected market resulting from sustained passenger traffic growth, the European rotorcraft manufacturers have decided to collaborate on the development of a civil tilt-rotor (CTR) suited for scheduled passenger transport missions. To achieve this goal, several critical technology projects, are being conducted within the 2000–2005 period. Among them was the Rotorcraft Handling, Interactions and Loads Prediction (RHILP), a European cooperative research program in the field of tilt-rotor aeromechanics and flight dynamics. RHILP commenced in March 2000 as part of the European Union's Fifth Framework Programme. The project involved a

Received 6 October 2004; revision received 9 May 2005; accepted for publication 16 May 2005.

*Research Associate, Flight Science and Technology, Department of Engineering; binoy@liv.ac.uk.
†Professor, Head, Department of Engineering; gareth.padfield@liv.ac.uk.
‡Senior Lecturer, Flight Science and Technology, Department of Engineering; d.j.walker@liv.ac.uk.

Fig. 1 Eurocopter's EUROTILT concept.

consortium of seven partners representing five EEC nations and was completed in April 2003.[1–3]

The main RHILP project objectives were to 1) define relevant handling qualities criteria for tiltrotor vehicles, 2) provide evidence of control-critical and load-critical aspects of tiltrotor flight, and 3) define active control solutions for load alleviation and control and stability augmentation. The present paper reports results from the study into active control for load alleviation. The critical loads are first discussed. Modeling aspects are reviewed and complementary active control solutions for rotor in-plane bending moments, gimbal flapping, and interconnect shaft torque are presented.

Modeling and Structural Load Alleviation

Before discussing the various aspects of modeling the structural loads, a brief discussion of the FLIGHTLAB model of the EUROTILT (Fig. 1)—the tilt-rotor configuration used in this paper—is given.

FLIGHTLAB Model of the EUROTILT (F-EUROTILT)

During the RHILP project, parallel modeling and simulation activities were conducted within the HOST (Eurocopter) and FLIGHTLAB (Liverpool) environments, providing a degree of verification and validation activities. Manimala et al.[4] discussed the FLIGHTLAB implementation at Liverpool and Rollet et al.[5] discuss the HOST implementation at Eurocopter. The main characteristics of the F-EUROTILT model are as follows. The aircraft's three-bladed counter-rotating gimbal mounted prop-rotors are modeled as if rigid. The gimbals are modelled with torsional spring-damper components in pitch and roll. No individual blade flapping is modeled in the F-EUROTILT. The prop-rotor blades are further modeled with nonlinear, quasi-steady aerodynamics in table lookup form as functions of angle of attack and Mach number computed on equal-annulus blade segments. A three-state dynamic rotor inflow model was used. The wing/flap lift, drag, and pitching moment coefficients are defined as functions of angle of attack, nacelle angle, and flap setting. A rigid drive-train model and XV-15–like engine governor system were modeled. No aerodynamic interactions were modeled in the F-EUROTILT model.

Structural Load Alleviation

Preliminary results from the structural load alleviation (SLA) work package of the RHILP project are presented in Ref. 4. The paper addresses modeling aspects in some detail, which forms the foundation for both the FLIGHTLAB simulated XV-15 and the EUROTILT configurations. The primary focus of attention in Ref. 4 was the suppression of in-plane rotor yoke loads for longitudinal maneuvers in airplane mode. Multivariable control law design using μ-synthesis was used to develop controller schemes and load suppression of 80–90% was demonstrated using rotor longitudinal cyclic control, albeit at a 20–30% performance penalty. The suppression and performance impact predicted in Ref. 4 by the off-line simulations were broadly realized in piloted simulations for longitudinal maneuvers with amplitude and frequency content similar to that of the design cases. However, as the pilot explored the system behavior in "free flight," load amplification was experienced—particularly in lateral maneuvers when sideslip was allowed to develop. It was clear that lateral cyclic control would be required for suppression of loads for more general maneuvers. This paper continues with the progress on the active control of SLA and investigates some of the issues not addressed in Ref. 4, especially the buildup and control of loads for more general maneuvering. The torque split on the interconnecting drive shaft is also analyzed during an aggressive lateral maneuver.

Rotor Oscillatory Yoke Chord Bending Loads (In-Plane Moments)

Yoke chord bending is the term used to describe the moment generated at the root of a rotor blade associated with bending of the blades in the plane of the rotor disk. Large oscillatory in-plane rotor loads develop during maneuvers in airplane and conversion modes, due primarily to the significant lift forces acting in the plane of the rotor disk, on the highly twisted blades.

Neglecting the aerodynamic drag force, the in-plane load M_z at the blade root can be defined as

$$M_z = \int_0^R L \sin\phi r \, \mathrm{d}r \tag{1}$$

where R is the blade radius, L is the lift per unit span, and ϕ is the rotor inflow angle. Please see Fig. A1 in Appendix A for a description of the rotor inflow angle and the lift force.

In airplane mode, due to the high forward velocity, the angle of inflow, ϕ, is large, generating an in-plane force component, $L \sin\phi$. Even in steady flight, the large in-plane force component leads to relatively high levels of 1/rev aerodynamic in-plane moment at the blade root in the rotating blade system whenever the resultant airflow has a component in the plane of the rotor disk. During a pitch (or yaw) maneuver, the in-plane oscillatory loads are substantially higher than the steady-state values. During a pull-up maneuver, changes in the body-axis vertical velocity alter the incidence of the rotor inflow causing the rotor disk to flap in the direction of the fuselage pitch.

During pull-up and pushover maneuvers in airplane mode, the short period mode is excited, typically resulting in a large pitch rate overshoot, before the steady-state maneuver is reached. The short period mode is also characterized by significant changes in body-axis vertical velocity and velocity perturbations in the rotor plane, effectively acting as longitudinal cyclic inputs, which cause the rotor blade to flap in the direction of the aircraft pitch change. The applied aerodynamic moment is then greater than that required to precess the gimbaled rotor, leading to an increased flapping in the direction of motion. The excessive flapping can cause elastomeric flap bearing loads and rotor mast bending loads. The SLA controller developed in Ref. 4 was shown to reduce the in-plane load by forcing the rotor to flap against the pitch rate through the application of longitudinal cyclic control. It was noted that the magnitude of the longitudinal flapping is directly proportional to the applied cyclic angle.

The total angular velocity of the rotor blades is the sum of the fuselage pitch rate and the gimbal longitudinal flapping rate. This creates a large out-of-plane aerodynamic moment acting on the rotor. For gimbaled rotors it can be shown[6] that once-per-revolution chordwise bending moments are directly related to the out-of-plane (flap) moments on the rotor. Thus, the in-plane bending loads on a tilt-rotor in a pull-up maneuver are significant and can limit the maneuverability of the aircraft. King et al.[7] report that the endurance limit of the rotor yoke is reached with a combined pitch rate of slightly less than 25 deg/s at an airspeed of 300 kn for the V-22 (i.e., load factor of about 6).

Effect of Body-Axis Vertical Velocity

The tangential and the normal relative wind velocities for a blade element on the right rotor, for a purely longitudinal maneuver, can be written as

$$u_t = u[a\sin(\psi) + b\cos(\psi)] + w\sin(\psi) + r_b\Omega$$

$$u_p = u - wa - r_b[q\cos(\psi) + \dot{a}\cos(\psi) - \dot{b}\sin(\psi)] \tag{2}$$

It is assumed that the effects due to the q^*z_h, q^*x_h terms and the second-order terms are negligible. The equations leading to this are derived in Appendix A. Note that the azimuth angle ψ is measured positive in the counterclockwise direction for the right rotor. Figures B1–B4 provided in Appendix B illustrates the axis systems used for the derivation of the blade element velocities.

As the aircraft pitches up, the vertical velocity builds up and increases the tangential velocity, u_t, at $\psi = 90$. The increased tangential velocity decreases the inflow angle of incidence and causes a once-per-revolution variation in the in-plane velocity; hence, the lift is increased at $\psi = 90$. As a result, the rotor blades flap up at the bottom of the disk at $\psi = 180$. Hence, the large body-axis vertical velocity induced by the pull-up maneuver at high speeds results in the effect of the pitch rate and the flap rate occurring in the same direction. The rotor contributions to both pitch derivatives, M_w and M_q, are positive, that is, destabilizing.

Referring to Eqs. (A13) (see Appendix A), the change in angle of attack during a pure longitudinal maneuver, for a right-rotor blade element at an azimuth angle of ψ and at a radial location of r_b, is given by

$$\delta\alpha = \left[u_t \Big/ \left(u_t^2 + u_p^2\right)\right]\{\delta w a + w\delta a + [(u_p/u_t)(\delta w + u\delta a) - r_b\delta\dot{b}] \times \sin(\psi) + [(u_p/u_t)u\delta b + r_b(\delta q + \delta\dot{a})]\cos(\psi)\} \quad (3)$$

From Eq. (3) the predominant term that gives rise to the once-per-revolution-variation in angle of attack, and hence the in-plane load variations in a symmetric pull-up maneuver, is $[(u_p/u_t)(\delta w + u\delta a)]\sin(\psi)$. This variation can be canceled out by the application of combined longitudinal cyclic control. A small amount of differential lateral cyclic control is required to cancel out the cosine term.

Analytic Approximations to the Yoke Chord Bending for Control Synthesis

Miller and Ham[6] arrived at the following expression for the perturbation in rotor chord bending moment (in rotating blade axis) for a constant-velocity gimbaled rotor during a longitudinal maneuver in airplane mode:

$$\delta M_z = \{k_1[2I_\beta\Omega(q + \dot{a}) + K_\beta b] + k_2\theta_{1s} + k_3\delta w\}\sin(\psi) + \{k_1[2I_\beta\Omega(r + \dot{b}) + K_\beta a] + k_2\theta_{1c}\}\cos(\psi) \quad (4)$$

where I_β is the flapping moment of inertia of the rotor blade, Ω is the rotor speed, and a and q are the gimbal longitudinal flap and aircraft pitch rate, respectively. The constants k_1, k_2, and k_3 are defined for a particular aircraft configuration and flight condition.

For a longitudinal maneuver, the most significant term in the in-plane moment expression is given by the aerodynamic moment balancing the gyroscopic moment acting on the gimbal:

$$\delta M_z = 2I_\beta\Omega(q + \dot{a})\sin(\psi) \quad (5)$$

Figure 2 shows a linear correlation between the peak in-plane load and the total angular rate. The data are obtained from FLIGHTLAB simulations of the EUROTILT at 200 kn equivalent airspeed (EAS) and 3000 m altitude with the stability and control augmentation disengaged. The range of total gimbal pitch rate has been deliberately exaggerated (compared with the maneuver envelope of a CTR) to highlight the linearity even for large-amplitude maneuvers.

For the design of SLA controllers it is necessary to develop linearized equations relating the controlled variable (in-plane bending) to available measurements and controls. Attempts were initially made to extract linear output equations for the in-plane loads from the nonlinear FLIGHTLAB model through numerical differencing of the output function representing the in-plane loads in the rotating blade axes system. This procedure led to inaccurate predictions due to the periodic nature of the individual blade moments. Hence, a new approach was used that makes use of multiblade coordinate (Coleman) transformation[8,9] to convert the in-plane loads from the individual blade coordinates to a hub-fixed coordinate frame. In multiblade coordinates, the loads have a period of 3/revolution on EUROTILT, but many of these combined effects cancel out. The dominant effect is the quasi-steady nonoscillatory envelope during maneuvers. The individual-blade in-plane loads $M_{z_{b1}}$, $M_{z_{b2}}$, and

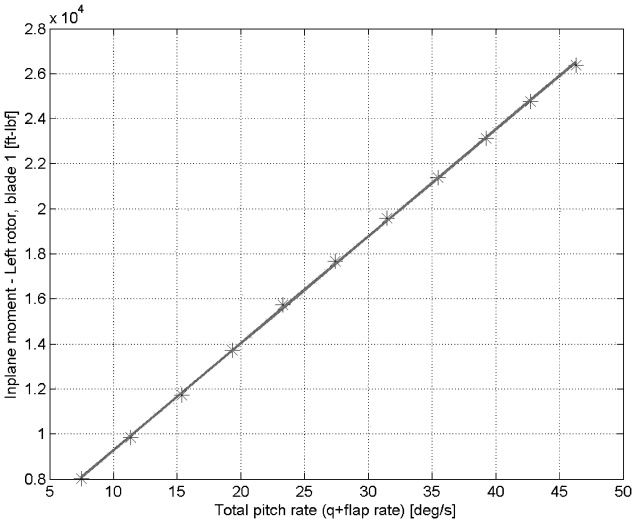

Fig. 2 Correlation of peak in-plane load with total rotor pitch rate.

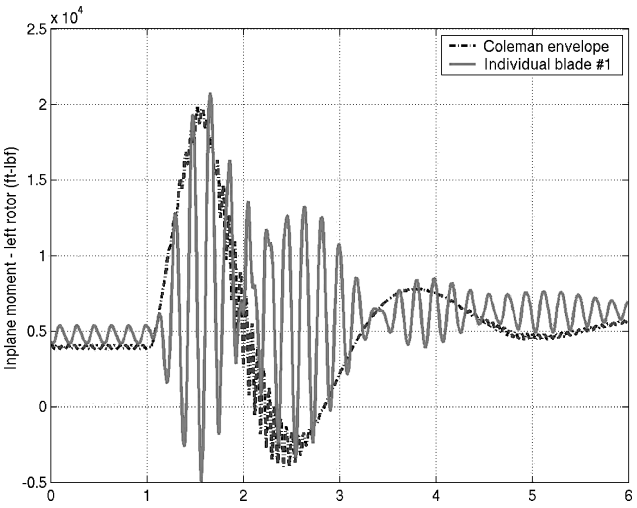

Fig. 3 In-plane moment blade root for a 2.5*g* pull-up maneuver (EUROTILT).

$M_{z_{b3}}$, at the root of each of the three blades, are transformed into a load envelope in multiblade coordinates using the transformation

$$\begin{bmatrix} M_{z_0} \\ M_{z_c} \\ M_{z_s} \end{bmatrix} = \frac{1}{3}\begin{bmatrix} 1 & 1 & 1 \\ 2\cos(\psi_1) & 2\cos(\psi_2) & 2\cos(\psi_3) \\ 2\sin(\psi_1) & 2\sin(\psi_2) & 2\sin(\psi_3) \end{bmatrix}\begin{bmatrix} M_{z_{b1}} \\ M_{z_{b2}} \\ M_{z_{b3}} \end{bmatrix} \quad (6)$$

where the azimuth angle for the ith blade is

$$\psi_i = \Omega t + (i - 1)2\pi/3 \quad (7)$$

The envelope of the load is the sum of the three first harmonic terms:

$$M_z = M_{z_0} + M_{z_c} + M_{z_s} \quad (8)$$

Figure 3 presents a comparison of the in-plane load envelopes in the multiblade and individual-blade coordinates for EUROTILT during a 2.5g pull-up maneuver. The multiblade approximation is considered sufficiently representative of the nonlinear blade load to be useful in the active control scheme.

In-Plane Loads in Sideslip

The preceding section described the in-plane load in airplane mode for pure longitudinal maneuvers and showed the effect of body-axis vertical velocity (incidence) buildup on the in-plane loads during pull-up maneuvers. In this section the effect of body-axis lateral velocity (sideslip) on the in-plane loads is described.

Effect of Body-Axis Lateral Velocity

Recalling the equations for the tangential and normal relative air velocities at a blade section for the right rotor from Appendix A and ignoring the pitch terms, we have

$$v^{\mathrm{bl}} = (u - r y_h)[a \sin(\psi) + b \cos(\psi)] + v \cos(\psi) + (w + p y_h) \sin(\psi) + r_b(\Omega + p)$$

$$w^{\mathrm{bl}} = (u - r y_h) - vb - (w + p y_h)a - r_b[r \sin(\psi) + \dot{a} \cos(\psi) - \dot{b} \sin(\psi)] \quad (9)$$

The velocity terms due to the x and z moment arms (pz_h and rx_h terms) and the second-order terms are neglected.

Examining Eqs. (9), it can be seen that the variation of the in-plane loads for lateral velocity v and the lateral gimbal flap is identical to the variation with respect to vertical velocity and longitudinal gimbal flap. Following similar arguments described in the preceding section, the change in angle of attack for a blade section on the right rotor due to lateral velocity, roll rate, and yaw rate buildup can be written as

$$\delta\alpha = \left[u_t \Big/ \left(u_t^2 + u_p^2\right)\right]\{[(u_p/u_t)\delta p r_b + \delta r y_h + b\delta v + \delta b v] + [(u_p/u_t)(u\delta a + \delta p y_h) + \delta r r_b - \delta \dot{b} r_b] \sin(\psi) + [(u_p/u_t)(u\delta b + \delta v) + \delta \dot{a} r_b] \cos(\psi)\} \quad (10)$$

Examination of Eq. (10) reveals that the once-per-revolution effect of the angle-of-attack change due to the lateral velocity can be canceled out by the application of combined lateral cyclic control. In addition to lateral cyclic, small amounts of differential longitudinal cyclic and differential collective control are required to cancel the effects of roll and yaw rates.

Simulation and Identification of In-Plane Loads for Yaw Rates

Figure 4 illustrates the response of the F-EUROTILT model to a pulse input in the rudder in airplane mode at the 200-kn EAS and 3000-m flight condition. Such an abrupt input in pedal is perhaps an unrealistic maneuver for a CTR in airplane mode. However, it is chosen to demonstrate the effect of yaw rate and lateral velocity on the rotor in-plane load.

The following observations can be made from Fig. 5:

1) There is a considerable increase in the in-plane moments as the body-axis lateral velocity builds up.

2) The left and right rotor gimbals tilt together toward the direction of the yaw rate.

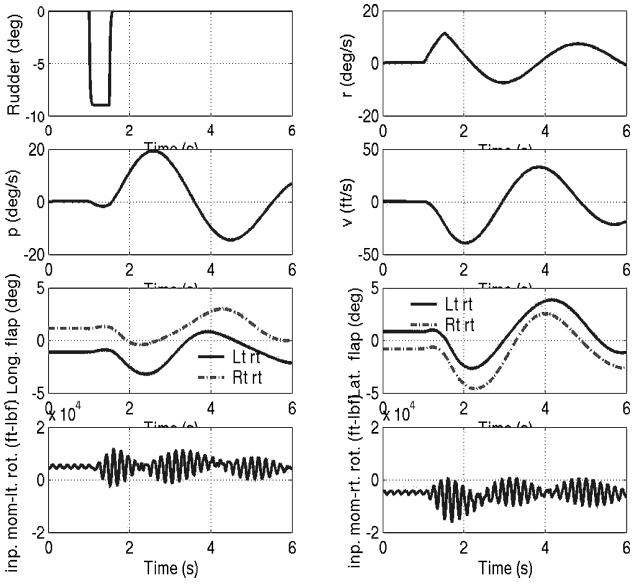

Fig. 4 Response of EUROTILT for a pulse input in rudder at 200-kn EAS at 3000 m.

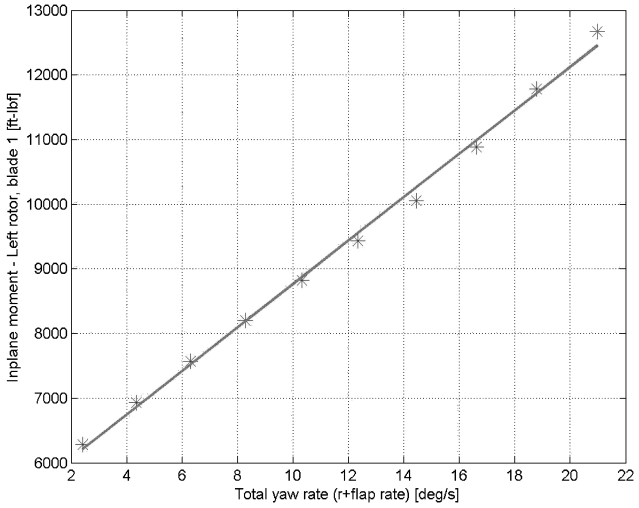

Fig. 5 In-plane moment peak vs yaw rate plus gimbal lateral flap rate.

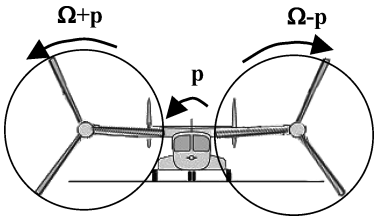

Fig. 6 Airplane-mode roll.

3) The left and right rotor gimbals tilt in opposite longitudinal directions ("nose down" or tilt forward for the right rotor and "nose up" or tilt back for the left rotor). Note that the hub–axis systems in FLIGHTLAB are such that a nose-up (tilt-back) longitudinal disk tilt is positive for the right rotor (counterclockwise) and negative for the left rotor (clockwise). The py_h terms in Eq. (10) have the effect of tilting the right-rotor gimbal in the nose-down direction and the left-rotor gimbal in the nose-up direction.

With reference to Eq. (4), it can be seen that the dominant term for the in-plane moment for a lateral maneuver is

$$2I_\beta \Omega (r + \dot{b}_2) \cos(\psi) \quad (11)$$

Figure 5 shows the variation of the peak in-plane moment against the sum of aircraft yaw rate and the lateral gimbal flap rate from the F-EUROTILT model with stability and control augmentation disengaged. The flight case is, once again, 200 kn EAS at 3000 m altitude. The range of total yaw rate has been deliberately exaggerated (compared with the maneuver envelope of a CTR) to highlight the linearity for large-amplitude maneuvers.

Interconnect Shaft Torque Split for Roll/Yaw Maneuvers

Effect of Roll Rate

In an airplane-mode roll maneuver, the aircraft rotational rate produces equal and opposite angular motions at the counter-rotating left and right rotors (Fig. 6) A roll to the right increases the rotation rate on the right rotor (after the rotor-speed governing effect has been applied) and decreases the rotation rate on the left rotor, resulting in a differential torque. For rapid roll maneuvers, this differential torque leads to high interconnect drive-shaft and mast torque, thereby reducing the fatigue life of the drive system mechanical components.

Examining the blade element equations in Appendix A shows that a positive roll leads to an increase in the tangential velocity for the blades on the right rotor and a decrease for the left-rotor blades. The increase in tangential velocity for the right-rotor blades decreases the angle of attack, α (decreases the inflow angle of incidence, ϕ), resulting in a higher torque from the right rotor. In a similar manner, the left-rotor torque is reduced, thus creating the torque split on the interconnecting drive shaft. Using the expression derived in

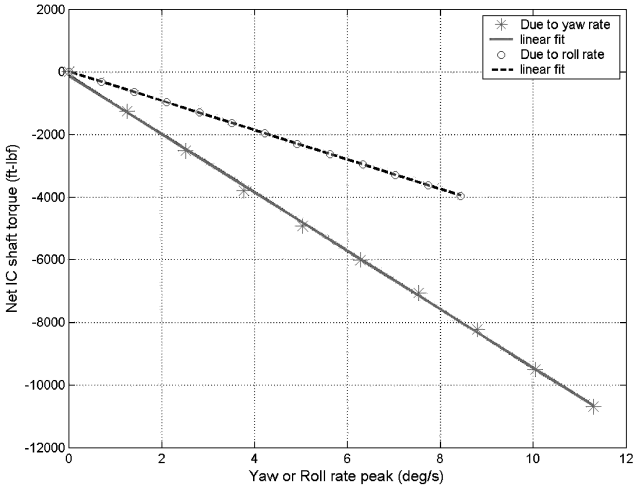

Fig. 7 Torque split vs peak of roll/yaw rate.

Appendix A for the blade element velocities, the change in angle of attack for a right-rotor blade element due to yaw and roll rate can be written as

$$\delta\alpha = \left[u_t \Big/ \left(u_t^2 + u_p^2\right)\right]\left[(u_p/u_t)\delta p r_b + \delta r y_h\right] \tag{12}$$

Effect of Yaw Rate

It may also be noted that yaw rate has an effect on the normal velocity component for a blade element section. A positive value of the yaw rate r leads to a decrease in the u_p term for the right rotor and an increase for the left rotor. This effect will also contribute to differential torques from the left and right rotors. Figure 7 shows the variation of the peak values of the net torque on the interconnect shaft against aircraft yaw/roll rate from the FLIGHTLAB EUROTILT model with stability and control augmentation disengaged. A strong linear correlation is shown between the peak torque split and the yaw/roll rate for the design case of 200 kn EAS at 3000 m altitude. The plots shows that the yaw rate has twice the effect on the torque split compared with the roll rate. Differential collective inputs are required to cancel out the effect of roll rate and yaw rate on the angle-of-attack changes.

Load Alleviation Control Concepts

The problem of prop-rotor SLA in aggressive pull-up maneuvers was addressed in the design of the automatic flight control system (AFCS) of the Bell-Boeing V-22 Osprey aircraft.[10] The oscillatory yoke chord-bending load limiter on this aircraft features modifications to the AFCS command model/stability compensation and rate limitation of the longitudinal stick command.

The SLA controller described in Refs. 6 and 11 used a modified eigenstructure assignment technique. Two different approaches to the development of control laws for rotor yoke chord load alleviation were investigated in Ref. 11. The first controller used flapping feedback to regulate longitudinal and lateral cyclic pitch angles, but because this compensator did not meet the stability robustness requirements, a second control system was developed using an eigenstructure assignment methodology. The resulting pitch rate feedback control law, which utilizes longitudinal cyclic pitch and elevator, provided a favorable match between the desired and achieved short-period eigenstructure and was robust to structural mode parameter uncertainties. The controller described in Ref. 6 utilized feedback of pitch rate, pitch angle, and normal velocity to generate control inputs on rotor cyclic pitch angles. As an observation, the study shows that the use of rotor flapping states in the feedback is not necessary for suppression of the in-plane loads. Stability robustness of the controller is demonstrated by means of singular value analysis where high-frequency modeling errors are represented as a multiplicative error at the system input.

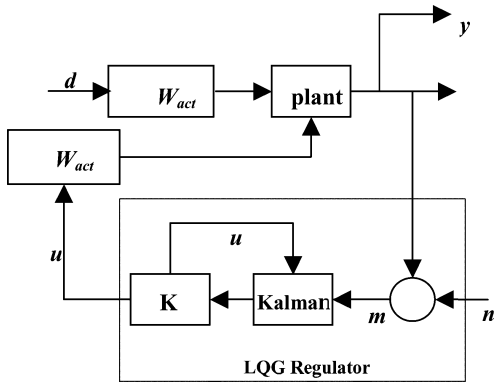

Fig. 8 LQG design for the SLA controller.

During the RHILP research reported in Ref. 4, the use of rotor cyclic control resulted in what were felt to be excessive excursions in gimbal longitudinal flapping. A complementary synthesis, using H-infinity techniques,[12] showed how the dual objectives of suppressing transient load and flapping during maneuvers were feasible when using both rotor cyclic and elevator controls. The effectiveness of the SLA controllers was investigated through piloted simulation trials at Liverpool with the full-envelope nonlinear FLIGHTLAB simulation model of EUROTILT, incorporating the combined Eurocopter stability augmentation system (SAS) and Centro Italiano Ricerche Aerospaziali (CIRA)/Liverpool SLA systems. As noted earlier in this paper, the suppression and performance impact predicted by the off-line simulations have been broadly realized for longitudinal maneuvers with amplitude and frequency content similar to that of the design cases. The controller was not, however, designed to do anything other than demonstrate a concept in longitudinal maneuvers.

Ideal SLA Controller for Airplane Mode

This section summarizes the control concepts previously described to alleviate the buildup of structural loads during airplane-mode maneuvers using rotor cyclic control. Attempts are made to obtain an "ideal" controller, which essentially cancels out the angle-of-attack changes in a maneuver (Fig. 8).

The concepts described in this section are perhaps less practicable in terms of a realizable SLA control system due to the unavailability of sensor measurements and the amount of blade pitch actuator authority required in airplane mode. However, the main idea behind such an ideal controller is to obtain insight into the physical mechanisms that cause the structural load buildup during airplane-mode maneuvers for a tilt-rotor.

Controller Design Process

The design is based on a 17-state linear model of EUROTILT at a straight-and-level reference trim condition of 200 kn EAS and a pressure altitude of 3000 m. The linear model contains the nine rigid-body states plus the longitudinal and lateral gimbal flap states and their rates for the left and right rotors. All the blade cyclic controls were assumed to be available for load alleviation in airplane mode. Hence, the vector $\boldsymbol{u}$ consists of the cyclic controls typically used in a tilt-rotor, given by

$$\boldsymbol{u} = [\theta_{0d}, \theta_{1c}, \theta_{1cd}, \theta_{1s}, \theta_{1sd}]$$

The feedback measurement signals were chosen as follows:

$$\boldsymbol{m} = [u, v, w, p, q, r, b_1, b_2, a_1, a_2]$$

The output vector for minimization consists of the multiblade in-plane moment envelopes of the left and right rotor, the torque split on the interconnecting shaft drive, and the lateral and longitudinal gimbal flap for the left and right rotors; thus,

$$\boldsymbol{y} = [M_{z1}, M_{z2}, Q_{\text{ts}}, b_1, b_2, a_1, a_2]$$

The disturbance vector contains the pilot inputs in all three axes for airplane mode, namely, aileron, elevator, and rudder:

$$\boldsymbol{d} = [\xi, \eta, \zeta]$$

A covariance value of 10^{-3} was used for modeling measurement noise. Actuator bandwidth of 60 rad/s was assumed:

$$W_{\text{act}} = 60/(s + 60)$$

The LQG design process involves the following steps:

1) Design of a full-state feedback gain ($\boldsymbol{K}$) that minimizes a linear quadratic performance measure of the form

$$\boldsymbol{J} = \int_0^\infty \{\boldsymbol{Qy}^2 + \boldsymbol{Ru}^2\}\,\mathrm{d}t \tag{13}$$

where $\boldsymbol{Q}$ and $\boldsymbol{R}$ are the weighting matrices chosen by the designer so that a reasonable tradeoff between performances and control authority is obtained. In addition, the elements of $\boldsymbol{Q}$ can be chosen such that a tradeoff between the performance of the different output variables can be obtained.

2) Design a Kalman filter that estimates the state vector given the measurements $\boldsymbol{m}$.

3) Connect the state feedback gain matrix K and the Kalman state estimator to form the LQG regulator.

The aforementioned process (using the MATLAB control systems toolbox) led to a 25-state, 10-input, 5-output controller. No attempt was made to obtain a reduced-order controller or to reduce the number of measurements available. Previous work[4] addressed the design of a robust controller with uncertainties, handling quality degradations, and sensor and actuator limitations in mind. In this paper uncertainties were not accounted for during the synthesis phase. The primary objective was to establish the feasibility of designing a controller that simultaneously minimized the in-plane moment, torque split, and the flap excursion during longitudinal and lateral maneuvers by using all of the available cyclic blade pitch actuations. The output from such a controller can be envisaged as an ideal set of control objectives that can be theoretically obtained; this forms the basis for comparison with a more robust and practical SLA controller. The results support the theoretical analysis and also provide an insight into the amount and type of cyclic pitch augmentation required to suppress the loads in airplane mode.

Performance of the LQG Controller

Principally, the SLA controller reduces the in-plane load by forcing the rotor to flap against the pitch rate through the application of longitudinal cyclic control. The use of longitudinal cyclic control was found to be an effective way of reducing the in-plane load during pitch maneuvers in airplane mode with small-to-moderate penalties on handling performance. However, longitudinal gimbal flap angles of magnitude similar to that of the applied cyclic were induced by the SLA system. It was noted that the magnitude of the longitudinal flapping was directly proportional to the applied cyclic angle.[4] High gimbal flapping is also a concern in tilt-rotor aircraft because this can lead to high elastomeric bearing and mast-bending loads. Hence, the reduction of gimbal flap is also included as a controller objective. It is possible to obtain a tradeoff between the flap excursion and the suppression of in-plane load with the inclusion of the flap angles in the objective function. This tradeoff is obtained by appropriately weighting the diagonal element of $\boldsymbol{Q}$ in Eq. (13). It is possible to obtain a controller that almost completely eliminates the flap excursions but produces reduced in-plane reduction and vice versa. The results presented in this paper were obtained by using a controller synthesized by a series of trial-and-error iterations on the elements of $\boldsymbol{Q}$ and $\boldsymbol{R}$ until a reasonable tradeoff between the in-plane load suppression and flap reduction was achieved. Note that the tradeoff is simply obtained by a visual inspection of the closed-loop time response of the system for control inputs.

The response of the open- and closed-loop systems to an elevator pulse input at the design point of the controller, with the SAS disengaged, is shown in Fig. 9. The figure shows the in-plane load envelope and the flapping behavior with and without the SLA controller. A near elimination of the in-plane loads and a longitudinal flap suppression of more than 3 deg is evident from the plot for this kind of pitch maneuver.

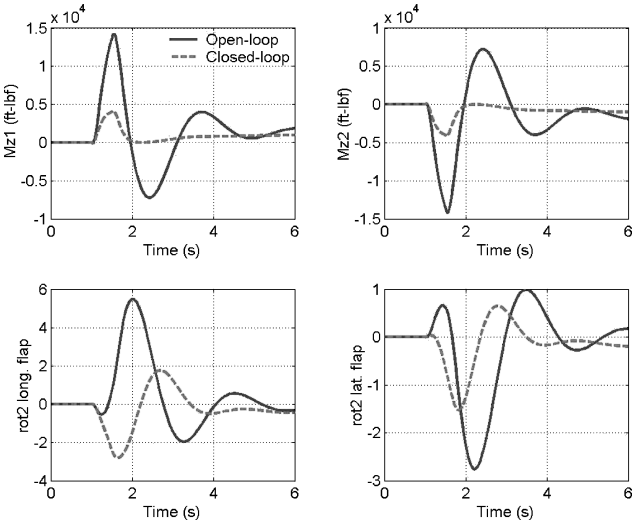

Fig. 9 Loads of EUROTILT to elevator pulse input at 200-kn condition.

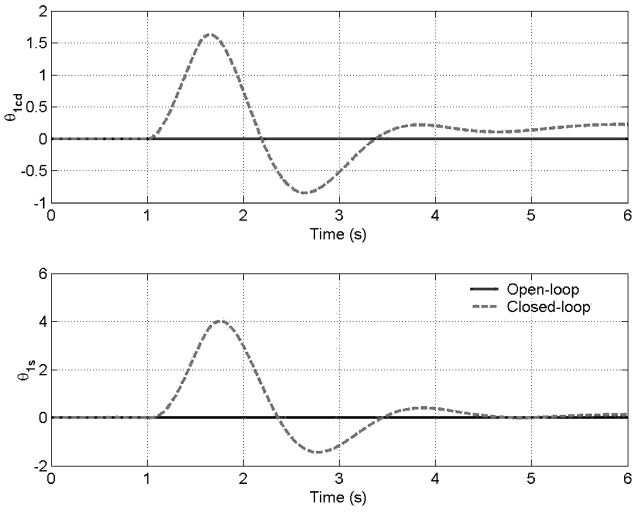

Fig. 10 Controller output for elevator pulse input at 200-kn condition.

The controller actions are shown in Fig. 10. A maximum of 4 deg combined longitudinal cyclic angle is commanded by the controller. In addition, approximately 2 deg of differential lateral cyclic angle is applied by the controller. Note that the differential lateral cyclic control applies equal amounts of lateral cyclic control on the left rotor (clockwise) and the right rotor (counterclockwise), causing them to tilt in opposite lateral directions.

Finally, the flight-path angle and pitch rate responses with and without the SLA, shown in Fig. 11, give some qualitative indication of the reduction in performance for the same pilot command. Fig. 12 shows the responses of the system for a pulse input in rudder with and without the SLA controller. It can be seen that an almost complete attenuation of the in-plane load and the torque split on the interconnecting shaft is obtained as a result of the controller actions. Inspection of the gimbal flap angles shows that a reduction of more than 1 deg in lateral flap is achieved.

The controller outputs for the rudder pulse input are shown in Fig. 13. The figure shows that a maximum differential collective input of 0.15 deg is sufficient to suppress the torque differences between the left and right rotors. It may be noted that the lateral cyclic angle profile is very similar to the body-axis lateral velocity. The

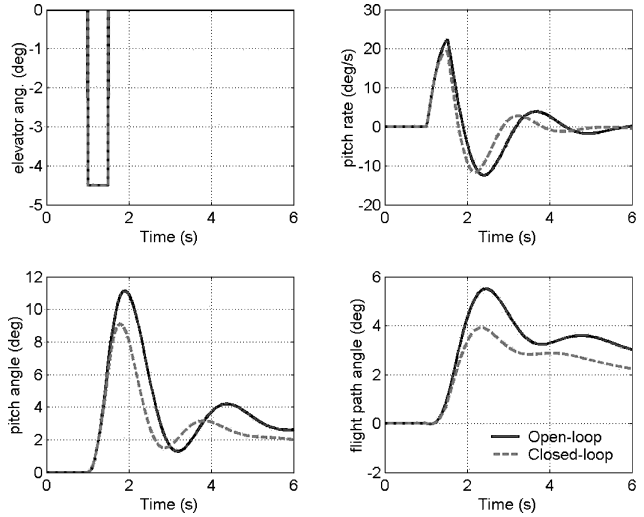

Fig. 11 Response of EUROTILT to elevator pulse input at 200-kn condition.

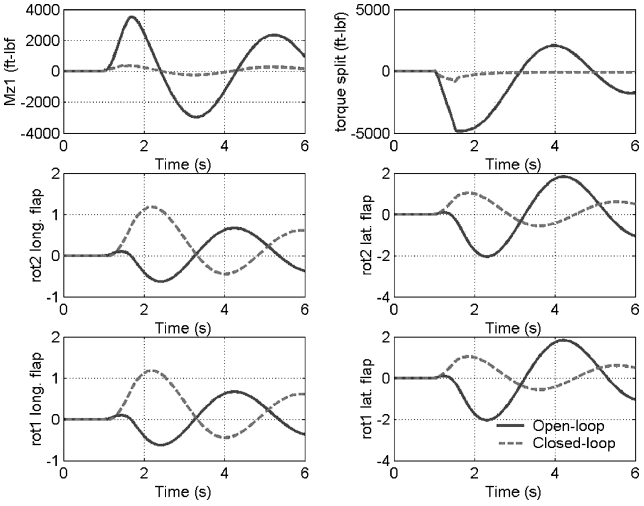

Fig. 12 Loads of EUROTILT to rudder pulse input at the 200-kn condition.

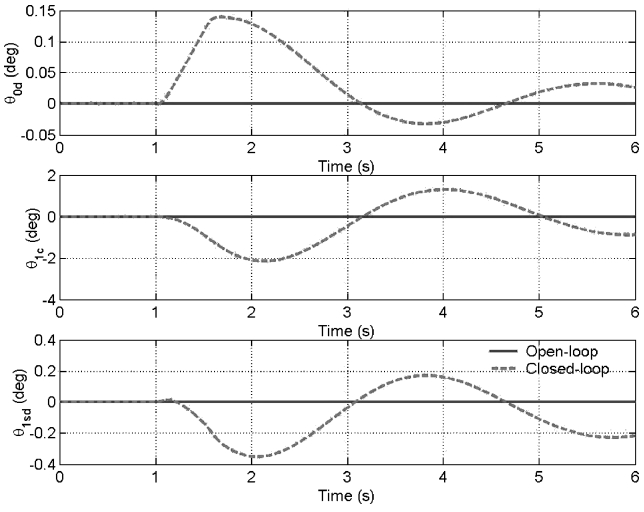

Fig. 13 Controller outputs for rudder pulse input at the 200-kn condition.

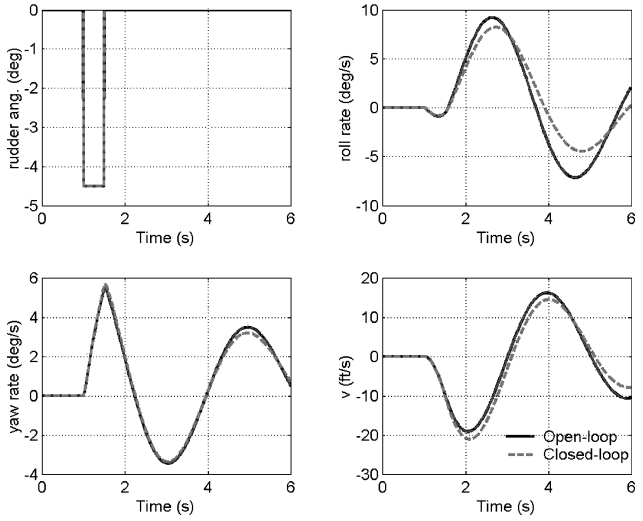

Fig. 14 Response of EUROTILT to rudder pulse input at the 200-kn condition.

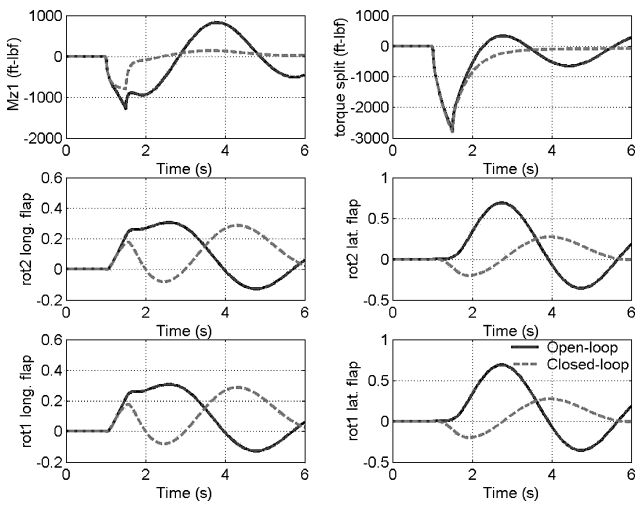

Fig. 15 Loads of EUROTILT to aileron pulse input at the 200-kn condition.

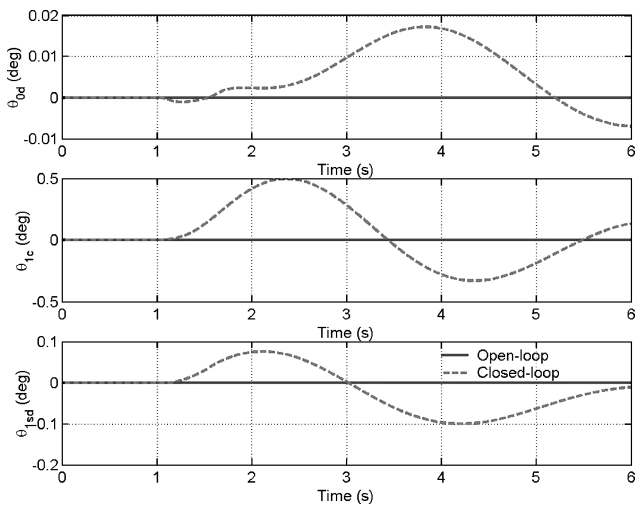

Fig. 16 Controller output for aileron pulse input at the 200-kn condition.

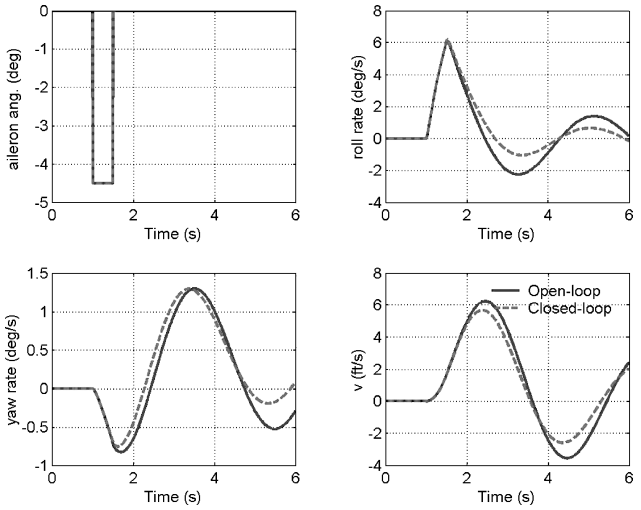

Fig. 17 Response of EUROTILT to aileron pulse input for 200-kn condition.

controller attempts to cancel out the change in angle of sideslip due to lateral velocity buildup by the application of the lateral cyclic angle. The controller also inputs a small amount of differential longitudinal cyclic control. It can be seen from Fig. 14 that the controller had very limited impact on the primary vehicle responses.

The responses of the open- and closed-loop systems for a pulse input in aileron are illustrated in Fig. 15. The open-loop responses suggest that the buildup of loads and flap angles is fairly benign for this type of input. The controller has failed to suppress the torque split through the application of differential collective; however, a reduction in flapping angles is obtained. Inspection of the control outputs (Fig. 16) suggests that the controller starts to input cyclic angles as the sideslip velocity builds up, resulting in reduced loads and flap response. The controller has failed to respond to the sudden roll rate buildup after the application of the aileron input and, hence, no reduction in torque split occurs. Finally for this case, the fuselage states are shown in Fig. 17.

Conclusions

This paper has presented an analysis of the structural loads of a tilt-rotor aircraft maneuvering in airplane mode and the potential for their suppression through active control. The study has addressed modeling aspects, particularly the nature of the buildup of dynamic loads during maneuvers. The FLIGHTLAB Eurocopter EUROTILT configuration has been used as the test aircraft. Mathematical analysis and simulation of the in-plane moments and gimbal flapping during longitudinal and lateral maneuvers is presented. The problem of the effect of torque split on the interconnect drive shaft in airplane mode for maneuvers, involving large roll and yaw rates, is also addressed. Attempts were made to obtain an "ideal" controller that simultaneously minimizes the gimbal flap excursions and the loads using an LQG formulation. In this preliminary multiobjective study, no consideration was given to robustness, actuator requirements, or the availability of measurements. The main objective of the controller design study was to investigate the effectiveness of cyclic controls to suppress the loads and flapping. The main conclusions that can be drawn from this study are as follows.

Evaluations performed using the controller show that use of cyclic controls is very effective in suppressing the buildup of in-plane loads and flap and interconnect drive-shaft torque split.

For pure longitudinal maneuvers, approximately 2 deg of lateral cyclic angle was required, in addition to the 4 deg longitudinal cyclic angle commanded by the controller, to achieve substantial load and flap reductions. A maximum of 2 deg lateral cyclic angle and 0.15 deg differential longitudinal cyclic angle was found to be sufficient for alleviating the in-plane loads and torque split for large-yaw maneuvers.

The torque split on the interconnect drive shaft has been analyzed and shown to be more severe when the aircraft maneuvers in yaw, in comparison to a similar amount of roll motion.

Although the LQG controller was effective in reducing the torque split for a high-yaw-rate maneuver, it failed to reduce the torque split for a roll rate maneuver. The reasoning behind this is not wholly clear. A possible solution for this is to remove the torque split minimization criteria from the objective function of the LQG design and address this issue as a separate problem. A simple feedback controller, which computes the differential collective requirement based on the yaw rate and roll rate, can be synthesized to minimize the torque split.

The LQG controller designed in this work had 25 states and several feedback channels, which poses several practical implementation issues. It may be possible to design lower order controllers with simpler feedback arrangements and obtain adequate performance and robustness criteria.

Appendix A: Gimbal Dynamics in Airplane Mode

In FLIGHTLAB, the gimbal is modeled by the use of two identical (in terms of their stiffness and damping values) torsional spring damper components placed such that one of them allows deflection in the roll axis and the other one in the pitch axis. These torsional springs, which allow deflections about the hub x and y axes, are also free to rotate with the hub. For a constant-velocity joint (homokinetic), the drive component is connected after the gimbal springs so that there is no cyclic variation of the rotor angular velocity. Hence, the transformation matrix from the hub-axis to the rotating blade axis can be written as

$$T_{\text{htobl}} = \begin{bmatrix} \cos(\psi) & \sin(\psi) & 0 \\ -\sin(\psi) & \cos(\psi) & 0 \\ 0 & 0 & 1 \end{bmatrix} \begin{bmatrix} 1 & 0 & 0 \\ 0 & \cos(b) & \sin(b) \\ 0 & -\sin(b) & \cos(b) \end{bmatrix} \times \begin{bmatrix} \cos(a) & 0 & -\sin(a) \\ 0 & 1 & 0 \\ \sin(a) & 0 & \cos(a) \end{bmatrix} \tag{A1}$$

assuming that the gimbal angles are small, so that $\cos(a) = 1$, $\sin(a) = a$, $\cos(b) = 1$, $\sin(b) = b$, and $ab = 0$.

The transformation matrix now becomes

$$T_{\text{htobl}} = \begin{bmatrix} \cos(\psi) & \sin(\psi) & -a\cos(\psi) + b\sin(\psi) \\ -\sin(\psi) & \cos(\psi) & a\sin(\psi) + b\cos(\psi) \\ a & -b & 1 \end{bmatrix} \tag{A2}$$

Velocity of Blade Elements

The velocity of a blade element in the rotating blade axis system can be defined as

$$\begin{bmatrix} u^{\text{bl}} \\ v^{\text{bl}} \\ w^{\text{bl}} \end{bmatrix} = T_{\text{htobl}} \begin{bmatrix} u^h \\ v^h \\ w^h \end{bmatrix} + \boldsymbol{\omega}^{\text{bl}} \times \boldsymbol{r}^{\text{bl}} \tag{A3}$$

where superscript bl denotes a vector quantity in the rotating blade axis system, $\boldsymbol{\omega}^{\text{bl}}$ is the total angular velocity of the rotating blade axis, and $\boldsymbol{r}^{\text{bl}}$ is the position vector of a blade element in the blade axis. The velocity of the right-rotor hub for the chosen axis system in FLIGHTLAB is given by

$$\begin{aligned} u^h &= -(w + py_h - qx_h) \\ v^h &= v + rx_h - pz_h \\ w^h &= u - ry_h + q^* z_h \end{aligned} \tag{A4}$$

where u, v, and w are the body-axis velocities of the aircraft and x_h, y_h, and z_h are the distances of the hub from the aircraft c.g. Superscript h implies a hub-axis system.

The total angular velocity of the rotating blade axis system is given by

$$\boldsymbol{\omega}^{\mathrm{bl}} = \begin{bmatrix} \cos(\psi) & \sin(\psi) & b\sin(\psi) \\ -\sin(\psi) & \cos(\psi) & b\cos(\psi) \\ a & -b & 1 \end{bmatrix} \begin{bmatrix} 0 \\ \dot{a} \\ 0 \end{bmatrix} + \begin{bmatrix} \cos(\psi) & \sin(\psi) & 0 \\ -\sin(\psi) & \cos(\psi) & 0 \\ 0 & 0 & 1 \end{bmatrix} \begin{bmatrix} \dot{b} \\ 0 \\ 0 \end{bmatrix} + \begin{bmatrix} 0 \\ 0 \\ \Omega \end{bmatrix} + T_{\mathrm{htobl}} \begin{bmatrix} -r \\ q \\ p \end{bmatrix} = \begin{bmatrix} \omega_x^{\mathrm{bl}} \\ \omega_y^{\mathrm{bl}} \\ \omega_z^{\mathrm{bl}} \end{bmatrix} \tag{A5}$$

where

$$\begin{aligned} \omega_x^{\mathrm{bl}} &= \dot{a}\sin(\psi) + \dot{b}\cos(\psi) - r\cos(\psi) + q\sin(\psi) \\ &\quad + p[-a\cos(\psi) + b\sin(\psi)] \\ \omega_y^{\mathrm{bl}} &= \dot{a}\cos(\psi) - \dot{b}\sin(\psi) + r\sin(\psi) + q\cos(\psi) \\ &\quad + p[a\sin(\psi) + b\cos(\psi)] \\ \omega_z^{\mathrm{bl}} &= -b\dot{a} + \Omega - ra - qb + p \end{aligned} \tag{A6}$$

and the position vector of a blade element is given by

$$\boldsymbol{r}^{\mathrm{bl}} = \begin{bmatrix} r_b & 0 & 0 \end{bmatrix}' \tag{A7}$$

Substituting for $\boldsymbol{\omega}^{\mathrm{bl}}$, $\boldsymbol{r}^{\mathrm{bl}}$, and the hub velocities in Eq. (A3), the velocity of a blade element on the right rotor at an azimuth angle ψ and at a distance of r_b from the hub center is given by

$$\begin{aligned} u^{\mathrm{bl}} &= \left(u - ry_h + q^* z_h\right)[-a\cos(\psi) + b\sin(\psi)] - (v + rx_h - pz_p) \\ &\quad \times \sin(\psi) + (w + py_h - qx_h)\cos(\psi) \\ v^{\mathrm{bl}} &= \left(u - ry_h + q^* z_h\right)[a\sin(\psi) + b\cos(\psi)] + (v + rx_h - pz_p) \\ &\quad \times \cos(\psi) + (w + py_h - qx_h)\sin(\psi) \\ &\quad + r_b(\Omega + p - ar - qb - b\dot{a}) \\ w^{\mathrm{bl}} &= \left(u - ry_h + q^* z_h\right) - (v + rx_h - pz_p)b - (w + py_h - qx_h)a \\ &\quad - r_b\{r\sin(\psi) + q\cos(\psi) + p[a\sin(\psi) + b\cos(\psi)] \\ &\quad + \dot{a}\cos(\psi) - \dot{b}\sin(\psi)\} \end{aligned} \tag{A8}$$

Change in Angle of Attack in Maneuvers

Figure A1 shows the aerofoil and wind geometry of a blade section. The inflow angle of incidence, ϕ, and the angle of attack, α, are give by

$$\phi = \tan^{-1}(u_p/u_t) \tag{A9}$$

$$\alpha = \theta - \phi \tag{A10}$$

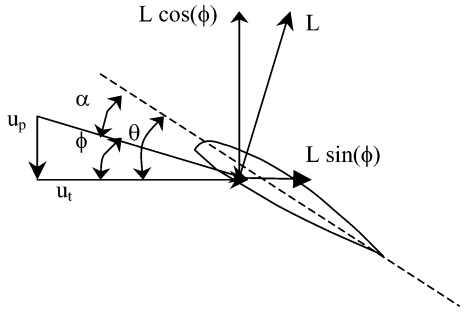

Fig. A1 A blade element.

Using the preceding equations and then using small-angle perturbation, the change in angle of attack on a blade element in a maneuver can be written as

$$\delta\alpha = \left[u_t \Big/ \left(u_t^2 + u_p^2\right)\right][(u_p/u_t)\delta u_t - \delta u_p] \tag{A11}$$

Using the expression derived for u_t (or v^{bl}) and u_p (or w^{bl}), the change in tangential and normal relative air velocities for a right-rotor blade element can be written as

$$\begin{aligned} \delta u_t &= u\delta a\sin(\psi) + u\delta b\cos(\psi) + \delta v\cos(\psi) \\ &\quad + \delta w\sin(\psi) + \delta p y_h\sin(\psi) + \delta p r_b \\ \delta u_p &= -\delta r y_h - (b\delta v - \delta b v) - \delta w a - \delta a w - r_b\delta r\sin(\psi) \\ &\quad - r_b\delta q\cos(\psi) - r_b\delta\dot{a}\cos(\psi) + r_b\delta\dot{b}\sin(\psi) \end{aligned} \tag{A12}$$

It is assumed that $\delta u = 0$ and the second-order terms such as $\delta r\delta a$, $\delta p\delta a$, and so on are negligibly small. Substituting for δu_t and δu_p in the change in angle of attack for a right-rotor blade element, the change in incidence can be written as

$$\begin{aligned} \delta\alpha &= \left[u_t \Big/ \left(u_t^2 + u_p^2\right)\right]\{[(u_p/u_t)\delta p r_b + \delta r y_h + b\delta v + \delta b v + a\delta w \\ &\quad + \delta a w] + [(u_p/u_t)(u\delta a + \delta w + \delta p y_h) + \delta r r_b - \delta\dot{b} r_b]\sin(\psi) \\ &\quad + [(u_p/u_t)(u\delta b + \delta v) + \delta q r_b + \delta\dot{a} r_b]\cos(\psi)\} \end{aligned} \tag{A13}$$

Appendix B: Axis Systems in FLIGHTLAB

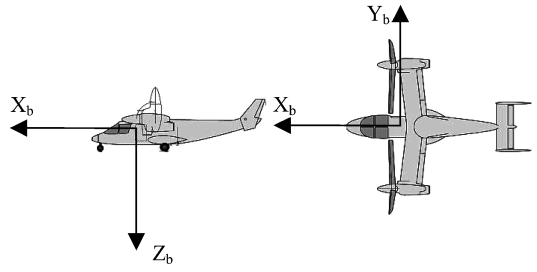

Fig. B1 FLIGHTLAB body-axis system.

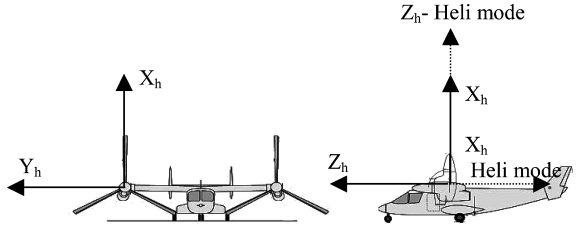

Fig. B2 Hub-axis system for the left and right rotors in airplane mode (dashed line for helicopter mode).

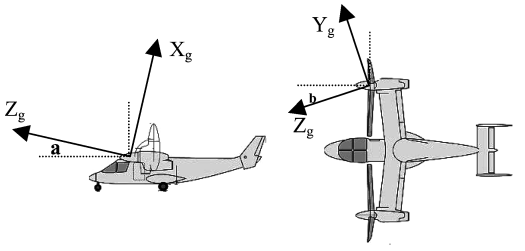

Fig. B3 Nonrotating gimbal axis system for the right rotor in airplane mode.

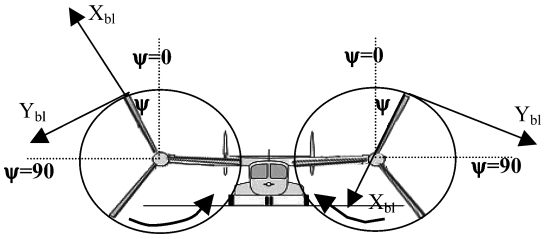

Fig. B4 Left- and right-rotor rotating blade axes.

Acknowledgments

The work reported in this paper was conducted in the RHILP project, sponsored by the European Commission as part of the Fifth Framework Programme. Particular thanks are due to Philippe Rollet of Eurocopter for his leadership of the RHILP project. The members of the RHILP team involved with this activity are acknowledged but particular recognition is given to the contributions of Mauro Naddei (CIRA) and German Roth (Eurcopter Deutschland).

References

[1]Rollet, P., "RHILP—A Major Step for European Knowledge in Tiltrotor Aeromechanics and Flight Dynamics," Aeronautics Days 2001, The European Commission, Hamburg, Germany, 28–31 Jan. 2001.

[2]Meyer, M., and Padfield, G. D., "First Steps in the Development of Handling Qualities Criteria for a Civil Tiltrotor," *Journal of the American Helicopter Society*, Vol. 50, No. 1, 2005, pp. 33–45.

[3]Desopper, A., Heuze, O., Routhieau, V., Roth, G., Grunhagen, W., and Haverdings, H., "Study of the Low Speed Characteristics of a Tilt Rotor," *28th European Rotorcraft Forum*, Paper 16, 2002.

[4]Manimala, B., Padfield, G. D., Walker, D. J., Naddei, M., Verde, L., Ciniglio, U., Rollet, P., and Sandri, F., "Load Alleviation in Tilt Rotor Aircraft Through Active Control; Modelling and Control Concepts," *Aeronautical Journal*, Vol. 108, No. 1082, 2004, pp. 169–184.

[5]Rollet, P., Sandri, F., and Roudaut, T., "Latest European Achievements in Tilt Rotor Piloted Simulation and Handling Qualities Assessments," *29th European Rotorcraft Forum*, Paper 57, 2003, pp. 57-1–57-8.

[6]Miller, D. G., and Ham, N. D., "Active Control of Tiltrotor Blade In-Plane Loads During Maneuvers," *14th European Rotorcraft Forum*, Paper 59, 1988, pp. 59-1–59-20.

[7]King, D. W., Dabundo, C., and Kisor, R. L., "V-22 Load Limiting Control Law Development," *49th Annual Forum of the American Helicopter Society*, 1993, pp. 211–224.

[8]Coleman, R. P., and Feingold, A. M., "Theory of Self-Excited Mechanical Oscillations of Helicopter Rotors with Hinged Blades," NACA 1351, 1958.

[9]Padfield, G. D., *Helicopter Flight Dynamics*, Blackwell Science, Oxford, 1996.

[10]Goldstein, K., and Dooley, L., "V-22 Control Law Development," *42nd Annual Forum of the American Helicopter Society*, 1986, pp. 673–684.

[11]Miller, D. G., Black, T. M., and Joglekar, M., "Tilt Rotor Control Law Design for Rotor Loads Alleviation Using Modern Control Techniques," *American Control Conference*, Vol. 3, 1991, pp. 2488–2495.

[12]Skogestad, S., and Postlethwaite, I., *Multivariable Feedback Control*, Wiley, Chichester, U.K., 1996.